Solar light and metal-doped TiO$_2$ to eliminate water-transmitted bacterial pathogens

Photocatalyst characterization and disinfection performance

2

3 **Solar light and metal-doped TiO$_2$ to eliminate water-transmitted bacterial**

4 **pathogens: Photocatalyst characterization and disinfection performance**

5

6 Danae Venieri[a*], Antonia Fraggedaki[a], Maria Kostadima[a], Efthalia Chatzisymeon[a†], Vassilios

7 Binas[b], Apostolos Zachopoulos[b], George Kiriakidis[b, c], Dionissios Mantzavinos[d]

8

9 [a] School of Environmental Engineering, Technical University of Crete, GR-73100 Chania,

10 Greece.

11 [b] Institute of Electronic Structure and Laser (IESL), FORTH, Vasilika Vouton, GR-70013

12 Heraklion, Greece.

13 [c] Department of Physics, University of Crete, GR-70013 Heraklion, Greece.

14 [d] Department of Chemical Engineering, University of Patras, Caratheodory 1, University

15 Campus, GR-26504 Patras, Greece.

16

[*] Corresponding author. Tel: +302821037801; E-mail address: danae.venieri@enveng.tuc.gr

[†] Current address: Institute for Infrastructure and Environment, School of Engineering, The University of
Edinburgh, The King's Buildings, Edinburgh EH9 3JL, United Kingdom.

Abstract

The present study deals with the inactivation of *Escherichia coli* and *Klebsiella pneumoniae* in water by means of heterogeneous photocatalysis under simulated solar irradiation. For this purpose, novel Mn-, Co- and Mn/Co-doped TiO_2 catalysts were prepared. A straightforward, simple and inexpensive process has been developed based on a co-precipitation method for the synthesis of metal-doped catalysts, which were subsequently assessed in terms of their disinfection efficiency. The effect of various operating conditions, such as metal dopant (Mn-, Co- and Mn/Co), dopant concentration (0.02-1 wt%), catalyst concentration (25-250 mg/L), bacterial concentration (10^2-10^8 CFU/mL), treatment time (up to 60 min), toxic effects on bacteria and photon flux (4.93-5.8×10^{-7} einstein/(L.s)), was examined under simulated solar irradiation. Metal-doped TiO_2 samples were prepared reproducibly and doping shifted the optical absorption edge to the visible region. Their activity was superior to the respective of commercially available P25 titania. The reference strains of *E. coli* and *K. pneumoniae* proved to be readily inactivated during photocatalytic treatment of aqueous samples, since disinfection occurred rapidly (i.e. after only 10 min of irradiation) with the dopant concentration affecting the overall process to a certain extent. Disinfection follows a pseudo-first order kinetic rate in terms of both bacteria removal. Inactivation of the bacteria is attributed to the oxidative degradation of their cells and increase of their cell permeability and not to the potential toxicity of the metal-doped semiconductors, which did not exhibit any bactericidal properties. It has been shown that the improved activity of the Mn-, Co-, and binary Mn/Co doped TiO_2 is accredited to the fact that they can be activated in the visible part of the spectrum, in the absence of UV light (i.e. >420 nm).

1. Introduction

Occurrence of bacterial pathogens and faecal contamination in surface water may pose high health risks, as they are considered major agents of waterborne diseases. Given that potable water is an essential requirement, efficiency of disinfection techniques is imperative for the adequate inactivation of microorganisms and the protection of public health [1]. The most popular disinfection techniques nowadays involve chemical compounds, filtration or radiation (e.g. chlorination, ozonation, UV irradiation etc.), which may act by different means like inhibition of enzymatic activity or destruction of cellular components [2]. However, considerable disadvantages including toxic by-products generated during chlorination, high cost of ozonation and action limitation depending on source-water turbidity when UV irradiation is applied, have led to the development of alternative methods [3, 4].

Semiconductor photocatalysis has emerged as a promising technique for microbial inactivation in various aqueous matrices, including diverse types of bacteria, fungi, viruses, and spores [5-7]. Titanium dioxide (TiO_2) is widely used as a photocatalyst in these processes due to its high efficiency, low toxicity, physico-chemical stability and low cost [2, 6, 8, 9]. A drawback, regarding most commercially available TiO_2 catalysts, is that they are mainly active under UV spectral range because of the high required band gap energy (~3.2 eV) for excitation of the semiconductor. Therefore, the bactericidal potential of TiO_2 photocatalysis has been extensively studied with the use of UV light, which is a small fraction of the total solar-light spectrum, excluding solar source of energy, which is abundant and free of cost [5, 10-12].

For this purpose, over the last decade, research interest has been focused on the use of solar irradiation for photocatalysis and thus the exploitation of the visible light energy. The photocatalytic efficiency of TiO_2 has been improved by many different strategies, which have

67 been adopted for either morphological or chemical modifications of the catalyst [2, 8, 13].

68 The latter involve incorporation of additional components in the TiO_2 structure, like non-

69 metal or/and noble and transition metal deposition. Doping the TiO_2 by several metals such as

70 copper, cobalt, manganese, etc. broadens the absorption spectrum of these semiconductors

71 towards the visible light region, as new energy levels are formed between the valence and

72 conduction band [1, 12-19]. The nature and the amount of the doping agent usually play an

73 important role concerning the photocatalytic activity. On the other hand, some possible

74 limitations have been reported like photo-induced corrosion and promoted charge

75 recombination at some metal sites [2, 8, 20].

76 Up until now, various studies have been conducted in terms of the evaluation of

77 disinfection efficiency of doped catalysts during water treatment under visible light, using

78 mostly *Escherichia coli* as a model microorganism [3-5, 10, 14, 16, 18, 21-24]. In most cases,

79 inactivation of bacteria has been attributed to the decomposition of bacterial outer membrane

80 due to phospholipid peroxidation of the membrane, caused primarily by hydroxyl radicals,

81 generated during treatment [25-27]. Apart from *E. coli*, the information regarding the

82 behaviour of other bacteria is very limited. The bacterial content of water consists of many

83 groups and species, which exhibit variable tolerance in disinfection as a result of differences

84 in cellular structure. *Klebsiella pneumoniae* is considered as an emerging human pathogen

85 and can be transmitted through water consumption, but it has been merely studied as far as its

86 resistance against disinfection is concerned [28, 29].

87 In this perspective, the objectives of the present work were (i) to prepare novel cobalt- and

88 manganese-doped titania materials and investigate their structural properties, and (ii) to study

89 their potential to purify aqueous samples in terms of *E. coli* and *K. pneumoniae* reference

90 strains removal under solar radiation. For this purpose, several operating parameters were

91 investigated, namely catalyst type and loading, dopant concentration, initial bacterial

92 concentration, as well as photon flux, which typically influence disinfection effectiveness.

93 Furthermore, scanning electron microscopy (SEM) was employed to detect destruction of

94 cellular structure induced by photocatalysis.

95

96 **2. Experimental**

97

98 *2.1 Materials*

99 Titanium (IV) oxysulfate hydrate (TiOSO$_4$·xH$_2$O), manganese (II) acetate tetrahydrate

100 (Mn(CH$_3$COO)$_2$), cobalt (II) acetate tetrahydrate (Co(CH$_3$COO)$_2$) and ammonium hydroxide

101 (25% NH$_4$OH) purchased from Aldrich were applied. Commercially available titanium

102 dioxide (TiO$_2$ P25) was purchased from Degussa - Evonik Corp. (physicochemical

103 characteristics are anatase:rutile 75:25, particle size of 21 nm and BET area of 50 m^2/g) and

104 was used as benchmark.

105

106 *2.2 Preparation of metal-doped TiO$_2$*

107 A co-precipitation method was used to prepare metal-doped TiO$_2$ nanoparticles with molar

108 ratio in different concentrations in the range of 0.02 - 1 wt%. Doped titanium dioxide was

109 precipitated at pH ~7 from aqueous solution of TiOSO$_4$ titanium (IV) oxysulfate hydrate and

110 dopant (Mn or Co or Mn/Co) by the addition of ammonia. After aging the suspension

111 overnight, the precipitate was filtered and dried under air at 373K. The residue was crushed to

112 a fine powder and calcined in a furnace at 973 K for 3 h. More details can be found in

113 previous work [13].

114

115 *2.3 Catalyst characterization techniques*

Powder X-ray diffraction patterns were collected on a Rigaku D/MAX-2000H rotating anode diffractometer (CuKα radiation) equipped with the secondary pyrolytic graphite monochromator operated at 40 kV and 80 mA over the 2θ collection range of 10–80°. The scan rate was 0.05° s^{-1}. The average particle size (D in nm) of nanoparticles was calculated from the line broadening of the X-ray diffraction peak according to the Scherrer formula, as follows:

$$D = k\lambda/(\beta\cos\theta) \qquad (1)$$

where k is the shape factor (~0.9), λ is the wavelength of the X-ray radiation (1.54 Å for CuKα), β is the full width at half maximum (FWHM) of the diffraction peak measured at 2θ, and θ is the Bragg angle.

The phase content of TiO_2 samples was calculated using the formula:

$$\%f_A=[1/(1+1.265\times I_R/I_A)] \times 100 \qquad (2)$$

where f_A is the content of anatase, and I_A and I_R are the integrated intensities of the anatase (100) and rutile (110) peaks respectively.

The UV – Visible diffuse reflectance spectra of the final powders were measured on a Perkin Elmer LAMBDA 950 with $BaSO_4$, as reference standard. The diffuse reflectance spectra were plotted as the Kubelka – Munk function, F(R), versus wavelength based on the Kubelka – Munk equation:

$$F(R) = (1-R)^2/(2R) \qquad (3)$$

where the reflectance R = $R_{sample}/R_{reference}$. The band gaps were then determined from the Kubelka – Munk function and the Tauc plots.

Surface morphology and elemental analysis of the samples were carried out using scanning electron microscopy (SEM) and an energy dispersive spectrometer (EDS) on a JSM-6390LV instrument. The microscopic nanostructures were studied by transmission electron microscopy (TEM) working at 200kV (JEM-2100 instrument equipped with LaB6 filament).

141

142   *2.4 Disinfection experiments*

143   The bacterial strains used in the present study were *E. coli* ATCC 23716 (American Type

144   Culture Collection, Rockville, Md. USA) and *K. pneumoniae* NCTC 5056 (Public Health

145   England Culture Collections). Both reference strains were inoculated separately in 10 mL of

146   nutrient broth (HiMedia Laboratories) and grown overnight at 37°C. The concentration of

147   bacterial cells in the suspension was estimated measuring its optical density at 600 nm

148   (Shimadzu UV1240 spectrophotometer) where, according to McFarland scale, an absorbance

149   of 0.132 corresponds approximately to a cell density of 1.5×10^{8} CFU/mL. Plate counts were

150   also performed for accurate bacterial count. In each case, suspensions were properly diluted to

151   achieve the desired initial bacterial concentration, which was used for the subsequent

152   experiments.

153   Photocatalytic experiments were conducted in batch type, laboratory scale photoreactor.

154   Solar irradiation experiments were carried out in a solar radiation simulator system (Newport,

155   model 96000) equipped with a 150 W xenon ozone-free lamp and an Air Mass 1.5 Global

156   Filter (Newport, model 81094), simulating solar radiation reaching the surface of the earth at

157   a zenith angle of 48.2^{o}. According to the spectral irradiance data given by the manufacturer,

158   simulated solar radiation contains about 5% UV-A radiation, and 0.1% UV-B radiation, while

159   the filter cuts radiations with wavelengths lower than 280 nm. The incident radiation intensity

160   on the photochemical reactor in the UV region of the electromagnetic spectrum was measured

161   actinometrically using 2-nitrobenzaldehyde (Sigma-Aldrich) as the chemical actinometer [30,

162   31] and it was found to be 5.8×10^{-7} einstein/(L.s), which corresponds to an irradiance of

163   1.31×10^{-2} W/m^{2}. Additional runs were performed with (i) a 420 nm cutoff filter to remove all

164   the UV light (FSQ-GG420, 50.8 mm x 50.8 mm), (ii) filter (FSQ-ND02, 50.8 mm×50.8 mm,

165   80% transmittance at 632.8 nm) to reduce irradiance to $5.3 \ 10^{-7}$ einstein/(L.s), and (iii) filter

166 (FSQ-ND04, 50.8 mm×50.8 mm, 40% transmittance at 632.8 nm) to reduce irradiance to 4.93

167 10^{-7} einstein/(L.s). Reactions took place in an open, double-walled, cylindrical glass vessel

168 under continuous stirring.

169 In a typical run, the bacteria suspension was spiked in sterile water of 200 mL which were

170 then loaded in the reaction vessel with the appropriate amount of catalyst. The solution was

171 left in the dark under stirring for 20 min in order to equilibrate and then exposed to solar

172 irradiation; this moment was taken as the starting point (time zero) of the disinfection

173 experiment. Temperature was maintained at $25\pm2^{o}C$ with a temperature control unit. The

174 external reaction vessel was covered with aluminum foil to reflect irradiation exerting the

175 outer wall of the reaction vessel. At specific time intervals samples of about 1.5 mL of the

176 reaction solution were withdrawn and analyzed with respect to viable bacterial cells applying

177 conventional culture method. All disinfection experiments were performed in triplicate.

178 Disinfection rate was measured in terms of *E. coli* and *K. pneumoniae* inactivation. The

179 detection and enumeration of both bacteria in the solution were performed using the serial

180 dilution streak plate procedure. The media used in the study were HiCrome Coliform Agar

181 (HiMedia Laboratories) and M-FC agar M1124 (HiMedia Laboratories) for *E. coli* and *K.*

182 *pneumonia*, respectively. Incubation was performed at $37^{o}C$ for 20-24 h before viable counts

183 were determined.

184 SEM observation of bacterial cells was carried out before and after treatment in each case,

185 with the view to detect any destruction of cellular structure of reference strains induced by

186 photocatalysis.

187

188 **3. Results and discussion**

189

190 *3.1. Structural and optical properties of metal-doped TiO$_2$ nanoparticles*

191   The XRD patterns of Mn-, Co-doped TiO_2, and binary Mn/Co co-doped TiO_2 with dopant

192   concentrations in the solution ranging from 0.02 to 1% for Mn- and Co-doped and 0.04 to

193   0.1% for the binary Mn/Co co-doped, respectfully, calcined at 700^oC for 3 h, are shown in

194   Figure 1. Peak at 25.3^o corresponds to the crystal plane 101 of the anatase phase. When the

195   dopant concentration was in the range of 0.02 - 0.3 wt% the samples were monophasic with

196   only the anatase polymorph TiO_2 being detected. Catalysts with 1 wt% of Mn- and Co-

197   dopants, respectively exhibited a mixture of phases with both anatase and rutile. The peaks at

198   2θ values of 25.3, 37.6, 48.2, 53.9, 54.8, 62.7 and 75.2 corresponding to the (101), (004),

199   (200), (105), (211), (204) and (215) planes, respectively are all anatase signature peaks. No

200   obvious diffraction peaks attributed to MnO_2 or CoO_2 were observed at low dopants

201   concentrations. Results of the particle size and phase content are shown in Table 1.

202   Figure 2 shows the UV-VIS absorption as a function of wavelength for metal-doped

203   catalysts. Dopants at different concentrations caused considerable absorption shifts towards

204   the visible range (400-800 nm) in comparison to the absorption threshold of P25 at 400 nm.

205   Moreover, increasing the dopant concentration led to a significant decrease in the band gap

206   energy below the value of 3.2 eV, which is required for excitation of the commercial P25

207   (Table 2). The band gap energy ranged between 2.4 and 2.87 eV and 2.4 and 2.97 eV for Mn

208   and Co-doped catalysts, respectively. In the case of Co and Mn/Co-doped TiO_2, an extra sub-

209   band gap energy was recorded in the range 1.4-1.6 eV, depending on the dopant concentration

210   (Table 2). The new absorption shoulder of these catalysts at 400-800 nm, related to the

211   presence of dopant (Figures 2b and 2c), may play key role in enhancing the overall

212   photocatalytic activity within the visible range. The textural features of the catalysts were

213   investigated with SEM (images are not shown for the sake of brevity); no specific

214   morphology changes were detected, while the spherical shape particles of all the samples

215   demonstrated some degree of agglomeration and the diameter ranged from 0.1 to 40 μm.

216 TEM images of the 1 wt% Mn- and 1 wt% Co-doped TiO_2 nanoparticles (Figure 3) confirmed

217 the agglomeration of nanoparticles with size ranging between 35 and 45 nm, consistent with

218 XRD measurements.

219

220 *3.2. Photocatalytic disinfection*

221 *3.2.1. Effect of catalysts concentration*

222 Given that the concentration of catalyst in slurry photocatalytic treatment strongly affects

223 the overall process, preliminary runs were performed with both bacterial reference strains

224 testing different commercial and metal-doped TiO_2 loadings. Tested concentrations were in

225 the range 25-250 mg/L for *E. coli* and 100-250 mg/L for *K. pneumoniae*. Higher loadings

226 were selected for *K. pneumoniae*, since it is a bacillus with a prominent capsule, which

227 prevents cell destruction by bactericidal factors [28]. According to the results, increasing the

228 catalyst loading improved inactivation rates for both microorganisms. In the case of *E. coli*,

229 optimal inactivation rates (approximately 4-Log reduction within 5 min of treatment) were

230 achieved when catalysts loading was 100 mg/L, beyond which disinfection reached a plateau.

231 Generally, increasing the photocatalyst concentration leads in lower penetration of light into

232 the slurry, deteriorating disinfection efficiency [3]. Conversely, higher catalysts concentration

233 was required for satisfactory decrease of *K. pneumoniae* population. In the presence of 250

234 mg/L of various types of TiO_2 that were used in the present study, total bacterial killing was

235 recorded in almost 10 min with an initial bacterial density of 10^5 CFU/mL. Therefore, all

236 subsequent experiments were conducted using 100 mg/L and 250 mg/L of catalysts for *E. coli*

237 and *K. pneumoniae* treatment, respectively. Optimal catalyst loadings may vary among

238 studies as they depend on many parameters such as photocatalytic reactor geometry, light

239 intensity, type of photocatalytic reactor etc. Apart from the trivial reference of *K. pneumoniae*

240   in photocatalytic studies, inactivation of *E. coli* is usually achieved in the range of loadings

241   used in this work [2, 4, 22].

242

243   *3.2.2. Effect of catalyst type*

244   Bacterial inactivation was recorded only under solar irradiation, when destruction of the

245   cells occurred. Efficiency of the metal-doped TiO_2 catalysts was assessed during a series of

246   photocatalytic experiments, whose results are shown in Figures 4, 5 and 6. It is observed that

247   Mn- and Co-doped catalysts showed better photocatalytic effectiveness than the commercially

248   available P25, in terms of both bacteria inactivation (Figures 4 and 5). Although P25 TiO_2 is

249   well known for its high photoreactivity due to the slow recombination of the electron-hole

250   pair and large surface area [3], metal dopants improved the activity of catalysts considerably,

251   as bacteria killing took place in almost 10 min of treatment. Moreover, it was observed that

252   increasing the dopant concentration, disinfection efficiency was improved, while an increase

253   beyond 0.3 wt% did not show any significant enhancement of the process.

254   Comparing Mn- and Co-, their effect was dependent of the experimental conditions in

255   question and the type of the specific bacterial reference strains. In the case of *E. coli*, a 6-Log

256   reduction was recorded in 10 min of solar irradiation using 0.1 wt% Mn-doped catalyst.

257   Similar population reduction was achieved in longer treatment period (15 min) and at higher

258   dopant concentration (1 wt%) when TiO_2 was doped with Co. Lower metal quantities than the

259   aforementioned ones proved to be insufficient for total *E. coli* inactivation even after 30 min

260   of treatment. As far as *K. pneumoniae* inactivation is concerned (Figure 6) it is observed that

261   the 0.3 wt% Mn- and 1% Co-doped TiO_2 catalysts showed optimum photocatalytic

262   performance when compared to the others and disinfection took place after only 10 min of

263   treatment. Despite that this specific emerging pathogen is considered persistent during various

264   treatments and disinfection techniques, photocatalysis with metal-doped catalysts seems quite

265 promising, since it may demonstrate complete inactivation in short periods with initial cell

266 densities as high as 10^5 CFU/mL.

267   Findings of the current study highlight the acceleration of disinfection process when metal-

268 doped catalysts are employed. The higher concentrations of Co required is probably attributed

269 to the fact that as a transition metal, it may act as a recombination site for the photo-induced

270 charge carriers thus, lowering the quantum efficiency [8]. Fisher et al., who worked with *E.*

271 *coli* and *Enterococcus faecalis* reported more rapid inactivation of both species in the

272 presence of TiO_2 doped with 1 wt% copper under solar irradiation compared to the respective

273 performed with undoped catalyst [1]. The bacterium-killing efficiency of doped TiO_2 is

274 referred to a quite extended variety of microorganisms, including *Listeria monocytogenes*,

275 *Shigella flexneri*, *Vibrio parahaemolyticus*, *Pseudomonas aeruginosa* and many others,

276 highlighting the advantage of dopants application in photocatalytic treatments [6, 23, 25, 28].

277   In further experiments, Mn/Co co-doped TiO_2 nanoparticles were successfully prepared

278 and their disinfection potential was tested under solar irradiation with *E. coli* and *K.*

279 *pneumoniae* reference strains. Inactivation rates are shown in Figure 6. Co-doped catalysts

280 induced a more rapid total bacterial killing in comparison with those with single metal dopant

281 at respective concentration. Surprisingly, a 5-Log reduction of *K. pneumoniae* population was

282 recorded in 15 min with both co-doped TiO_2, while *E. coli* required 30 min for complete

283 elimination with the highest dopants concentration (0.1 wt%). Similar inactivation rates for *E.*

284 *coli* were observed in a relevant study, where TiO_2 nanoparticles co-doped with N and Ag

285 were used for disinfection under visible light irradiation [32]. In another case, the application

286 of N and S co-doped P25 resulted in a 4-Log *E. coli* inactivation after 90 min of exposure to

287 visible light [33]. According to the general observation, composite dopants can compensate

288 the disadvantages of the individual components, inducing a synergistic effect [2, 8].

289   In order to further investigate the destruction of cellular structure of reference strains

290   induced by photocatalysis, SEM was employed and selective images are shown in Figure 7.

291   During photocatalysis the first oxidative stress is caused to bacteria when the catalyst

292   nanoparticles interact with intact cells. The detrimental effect is expanded towards the

293   cytoplasmic membrane, increasing cell permeability and allowing the outlet of intracellular

294   components, which finally cause cell death [14, 25]. In many cases the resultant change in cell

295   permeability is confirmed by potassium ion (K^+) leakage [34]. In the case of *K. pneumoniae*

296   the remnants of polysaccharide capsules combined with material released from the cell are

297   visible (Figures 7h to 7j). The progressive massive generation of hydroxyl radicals during the

298   process overcomes any protection mechanism of bacterial cells, whose density in reaction

299   mixture decreases with increasing time (Figures 4-6). In the course of treatment inactivation

300   becomes slow, which, according to Vijay et al., is attributed to the protection provided to

301   remaining active cells by metabolites excreted from the destructed ones [4].

302

303   *3.2.3. Effect of initial bacterial concentration*

304   A series of experiments was carried out to assess bacterial inactivation as a function of

305   initial concentration of the cells in the reaction mixture. In general, an increase in bacterial

306   density led to a decrease in the inactivation. Retardation of disinfection was more

307   promounced in the case of *E. coli*. For instance, when initial concentrations were 10^4 and 10^6

308   CFU/mL the period for total bacterial killing was 15 and 30 min, respectively, while complete

309   inactivation was not achieved in the presence of higher concentration (10^8 CFU/mL), where

310   residual *E. coli* cells reached a plateau showing an overall decrease of 6 orders of magnitude.

311   The almost same trend was recorded for *K. pneumoniae*, which was inactivated in 10 and 15

312   min when starting concentrations were 10^2 and 10^3 CFU/mL, respectively.

313   Disinfection rates can be fitted satisfactorily to a pseudo-first order kinetic expression, as

314   can be seen in Figure 8; from the slopes of the resulting straight lines kinetic rate constants

315   were calculated at 0.53 (r^2=0.96), 0.83 (r^2=0.92) and 0.77 min^{-1} (r^2=0.80) for initial *E. coli*

316   concentration of 10^4, 10^6 and 10^8 CFU/mL, respectively. The corresponding values for *K.*

317   *pneumoniae* were 0.43 (r^2=0.92), 0.57 (r^2=0.95) and 1.08 min^{-1} (r^2=0.99) for initial

318   concentration of 10^2, 10^3 and 10^5 CFU/mL.

319   Usually, the disinfection ability of common techniques is inversely proportional to initial

320   bacterial concentration. However, the required time for total inactivation depends on the

321   tested bacterial species in each case. Residual cells of the reference strains after long

322   treatment periods (> 30min) when high initial densities were employed, may be explained by

323   the survival of a resistant subpopulation as a result of protection by clumping of

324   microorganisms or even by genetically conferred resistance [35].

325

326   *3.3 Why does doping enhance photocatalytic disinfection?*

327   Results of the present study highlight the superiority of metal-doped catalysts compared to

328   P25, in terms of bacterial removal in aqueous samples under simulated solar irradiation. In

329   this respect, an attempt was made to identify the likely reasons for the improved activity of

330   doped catalysts.

331   Firstly, a point of consideration should be the biocidal nature of the metals used for the

332   preparation of catalysts. In some cases, metal-doped catalysts induce cell destruction of

333   bacteria, due to the toxicity of metal ions released into the reaction solution [18]. This may

334   occur even at minute metal concentrations according to the oligodynamic effect [36].

335   Accordingly, in order to assess the instantaneous toxicity of the novel Mn- and Co-doped

336   catalysts to microorganisms during their treatment, a set of experiments was performed in the

337   dark with the catalysts which had the lowest (0.02%) and highest (1%) concentration of metal

14

338   dopants. The catalyst concentration in the aqueous solution was 250 mg/L and initial bacterial

339   concentration of both reference strains was 10^4 CFU/mL. Bacterial density of *E. coli* and *K.*

340   *pneumoniae* remained stable within the period of the treatment, which lasted almost 1 h. It is

341   clearly shown that the metal-doped catalysts were not toxic to the selected reference strains

342   regarding their short-term toxic effects. Many metals are toxic to microorganisms at micro- or

343   millimolar concentrations, resulting in the development of resistance mechanisms in

344   microbial cells. In the case of cobalt, it is required as a trace element in procaryotes and

345   eucaryotes to fulfill a variety of metabolic functions. At high intracellular concentration the

346   redox active metal ion Co^{2+} is highly toxic [37]. According to our results, no bacterial

347   inactivation was recorded in the presence of both catalysts, indicating that no stress was

348   induced in the cells during their exposure to both metals.

349   Secondly, doping shifted catalyst absorption to the visible region up to 600 nm, as well as

350   decreased the band gap energy as clearly shown in Figure 2 and Table 2. Therefore, it was

351   possible to use the main part of the solar spectrum and surpass one of P25 drawbacks, which

352   is its low activity beyond the range of UV light. To investigate this effect further, experiments

353   were performed using a filter to cut-off UV light below 420 nm. The exclusion of UV light

354   led to a considerable inactivation of bacterial populations, which was more pronounced in the

355   case of *E. coli.* Specifically, in the presence of 0.1 and 1 wt% of Mn- and Co-doped TiO$_2$ the

356   overall decrease of *E. coli* cells after 30 min of treatment was 74.3% and 94%, respectively

357   (data for *E. coli* and Mn are shown in Figure 9a; for the sake of brevity data with Co are not

358   shown). For the same period of time and with the use of 1 wt% Mn- and Co-doped TiO$_2$, the

359   respective inactivation of *K. pneumoniae* reached 28% and 44% (data for *K. pneumoniae* and

360   Co are shown in Figure 9b; for the sake of brevity data with Mn are not shown). Noticeably,

361   the commercial P25 catalyst exhibited no photocatalytic activity above 420 nm and bacterial

362   populations of both strains remained intact throughout the process (data not shown). The

363 metal-doped catalysts (0.1 wt% Mn and 1 wt% Co) showed satisfactory photocatalytic activity

364 within the visible spectral range of the provided irradiation, causing detrimental effects on the

365 bacteria, which partly inactivated the cells in the reaction mixture. Their efficiency was

366 improved with the addition of UV light, as bacterial populations reached zero levels within 10

367 min of treatment. The contribution of UV light to the overall photocatalytic activity is clearly

368 shown in Figure 9 as some experiments were also performed at reduced photon fluxes. Total

369 removal of *E. coli* and *K. pneumoniae* occurred within 10 min only at 5.8×10^{-7} einstein/(L.s),

370 while three-fold or even longer periods were required to achieve the same inactivation at 5.3

371 10^{-7} and 4.93×10^{-7} einstein/(L.s). The detrimental effect of decreasing flux to disinfection

372 performance was more pronounced in the case of *K. pneumoniae*, highlighting the resistant

373 nature of the strain.

374   These findings verify the fact that chemical doping may act as a satisfactory means for

375 sensitization of TiO_2 in the visible light region, which is responsible for the enhanced

376 photocatalytic activity recorded in this work. Moreover, dopants on the surface of TiO_2 may

377 act as an electron trap, thus promoting interfacial charge transfer and delaying the

378 recombination of the light-induced electron-hole pair [38], which also leads to enhanced

379 activity.

380

381 **4. Conclusions**

382 The present study focused on solar photocatalytic disinfection with the use of novel cobalt-

383 and manganese-doped titania materials and reference strains of *E. coli* and *K. pneumoniae*.

384 - Metal-doped TiO_2 was prepared successfully and doping shifted the optical absorption

385   edge to the visible region.

386 - Dopants significantly enhanced (by a factor of 2-3) the photocatalytic activity of TiO_2

387   under solar irradiation, in terms of both bacteria inactivation.

388   - Dopants concentrations affected the overall process up to a certain level, while an increase

389   beyond 0.3 wt% did not show significant enhancement of disinfection rates. It is implied

390   that doping levels >0.3 wt% introduce heavy modification of the TiO_2 semiconductor, thus

391   hindering the production/diffusion of charges under light and, consequently, precluding the

392   effective interaction of these charges to inactivate bacteria.

393   - Comparing Mn and Co dopants, their performance varied depending on operating

394   parameters, such as the reference strain and the initial bacterial concentration.

395   - All catalysts were effective for the removal of *K. pneumoniae*, which is considered as an

396   opportunistic pathogen highly resistant in various water treatments.

397   - The improved activity of metal-doped titania is accredited to the optical absorption shifts

398   towards the visible region and to the recombination delay of the electron-hole pair, since

399   metals did not exhibit any bactericidal properties and catalysts were considerably

400   sensitized in the absence of UV light.

401

406

References

[1] M.B. Fisher, D.A. Keane, P. Fernández-Ibáñez, J. Colreavy, S.J. Hinder, K.G. McGuigan, S.C. Pillai, Appl. Catal. B: Environ 130–131 (2013) 8–13.

[2] S. Malato, P. Fernández-Ibáñez, M.I. Maldonado, J. Blanco, W. Gernjak, Catal. Today 147 (2009) 1–59.

[3] R.P.S. Suri, H.M. Thornton, M. Muruganandham, Environ. Technol. 33 (2012) 1651–1659.

[4] M. Vijay, K. Ramachandran, P.V. Ananthapadmanabhan, B. Nalini, B.C. Pillai, F. Bondioli, A. Manivannan, R.T. Narendhirakannan, Curr. Appl. Phys. 13 (2013) 510–516.

[5] J.G. McEvoy, W. Cui, Z. Zhang, Catal. Today 207 (2013) 191–199.

[6] B. Wang, M.K.H. Leung, X.Y. Lu, S.Y. Chen, Appl. Energ. 112 (2013) 1190–1197.

[7] G. Veréb, L. Manczinger, A. Oszkó, A. Sienkiewicz, L. Forró, K. Mogyorósi, A. Dombi, K. Hernádi, Appl. Catal. B: Environ. 129 (2013) 194–201.

[8] M. Pelaez, N.T. Nolan, S.C. Pillai, M.K. Seery, P. Falaras, A.G. Kontos, P.S.M. Dunlop, J.W.J. Hamilton, J.A. Byrne, K. O'Shea, M.H. Entezari, D.D. Dionysiou, Appl. Catal. B: Environ. 125 (2012) 331–349.

[9] D. Dvoranová, V. Brezová, M. Mazúra, M.A. Malati, Appl. Catal. B: Environ 37 (2002) 91–105.

[10] H.U. Lee, S.C. Lee, S. Choi, B. Son, S.M. Lee, H.J. Kim, J. Lee, Chem. Eng. J. 228 (2013) 756–764.

[11] H. Feng, M.H. Zhang, L.E. Yu, Appl. Catal. A: Gen. 413–414 (2012) 238–244.

[12] Q.R. Deng, X.H. Xia, M.L. Guo, Y. Gao, G. Shao, Mater. Lett. 65 (2011) 2051–2054.

[13] V.D. Binas, K. Sambani, T. Maggos, A. Katsanaki, G. Kiriakidis, Appl. Catal. B: Environ. 113–114 (2012) 79–86.

432 [14] C. Karunakaran, G. Abiramasundari, P. Gomathisankar, G. Manikandan, V. Anandi, J.
433 Colloid Interf. Sci. 352 (2010) 68–74.

434 [15] J. Marugán, P. Christensen, T. Egerton, H. Purnama, Appl. Catal. B: Environ. 89 (2009)
435 273–283.

436 [16] C. Karunakaran, A. Vijayabalan, G. Manikandan, Res. Chem. Intermed. 39 (2013) 1437–
437 1446.

438 [17] N.G. Moustakas, A.G. Kontos, V. Likodimos, F. Katsaros, N. Boukos, D. Tsoutsou, A.
439 Dimoulas, G.E. Romanos, D.D. Dionysiou, P. Falaras, Appl. Catal. B: Environ. 130–131
440 (2013) 14–24.

441 [18] M.P. Reddy, A. Venugopal, M. Subrahmanyam, Water Res. 41 (2007) 379–386.

442 [19] K.B. Jaimy, S. Ghosh, K.G. Warrier, J. Solid State Chem 196 (2012) 465–470.

443 [20] V.C. Papadimitriou, V.G. Stefanopoulos, M.N. Romanias, P. Papagiannakopoulos, K.
444 Sambani, V. Tudose, G. Kiriakidis, Thin Solid Films 520 (2011) 1195–1201.

445 [21] G. Veréb, L. Manczinger, G. Bozsó, A. Sienkiewicz, L. Forró, K. Mogyorósi, K.
446 Hernádi, A. Dombi, Appl. Catal. B: Environ. 129 (2013) 566–574.

447 [22] L. Rizzo, D. Sannino, V. Vaiano, O. Sacco, A. Scarpa, D. Pietrogiacomi, Appl. Catal. B:
448 Environ. 144 (2014) 369–378.

449 [23] M.S. Wong, W.C. Chu, D.S. Sun, H.S. Huang, J.H. Chen, P.J. Tsai, N.T. Lin, M.S. Yu,
450 S.F. Hsu, S.L. Wang, H.H. Chang, Appl. Environ. Microbiol. 72 (2006) 6111–6116.

451 [24] C. Karunakaran , A. Vijayabalan, G. Manikandan, P. Gomathisankar, Catal. Commun. 12
452 (2011) 826–829.

453 [25] S. Swetha, S.M. Santhosh, R.G. Balakrishna, Photochem. Photobiol. 86 (2010) 1127–
454 1134.

455 [26] V.A. Nadtochenko, A.G. Rincon, S.E. Stanca, J. Kiwi, J. Photochem. Photobiol. A-
456 Chem. 169 (2005) 131–137.

19

457   [27] J. Kiwi, V. Nadtochenko, Langmuir 21 (2005) 4631–4641.

458   [28] R.L. Burke, C.A. Whitehouse, J.K. Taylor, E.B. Selby, Comparative Med. 59 (2009)

459   589–597.

460   [29] M. Wang, B. Cao, Q. Yu, L. Liu, Q. Gao, L. Wang, L. Feng, J. Clin. Microbiol. 46

461   (2008) 3555–3563.

462   [30] K.L. Willett, R.A. Hites, J. Chem. Educ. 77 (2000) 900–902.

463   [31] E.S. Galbavy, K. Ram, C. Cort Anastasio, J. Photochem. Photobiol. A-Chem. 209 (2010)

464   186–192.

465   [32] P. Wu, R. Xie, K. Imlay, J.K. Shang, Environ. Sci. Technol. 44 (2010) 6992–6997.

466   [33] J.A. Rengifo-Herrera, E. Mielczarski, J. Mielczarski, N.C. Castillo, J. Kiwi, C. Pulgarin,

467   Appl. Catal. B: Environ. 84 (2008) 448–456.

468   [34] Z. X. Lu, L. Zhou, Z. L. Zhang, W. L. Shi, Z. X. Xie, H. Y. Xie, D. W. Pang, P. Shen,

469   Langmuir 19 (2003) 8765–8768.

470   [35] R.M. Maier, I.L. Pepper, C.P. Gerba, Environmental Microbiology, second ed.,

471   Academic Press, Elsevier, 2009.

472   [36] S. Rtimi, M. Pascu, R. Sanjines, C. Pulgarin, M. Ben-Simon, J.C. Lavanchy, A. Houas, J.

473   Kiwi, Appl. Catal. B: Environ. 138–139 (2013) 113–121.

474   [37] C. Ranquet, S. Ollagnier-de-Choudens, L. Loiseau, F. Barras, M. Fontecave, J. Biol.

475   Chem. 282 (2007) 30442–30451.

476   [38] W. Wang, J. Zhang, F. Chen, D. He, M. Anpo, J. Coll. Interf. Sci. 323 (2008) 182–186.

477 **Table 1.**

478 Average particle size and phase composition for Mn-, Co- and Mn/Co-doped TiO$_2$ catalyst.

Dopant concentration (molar ratio)	Mn-doped TiO$_2$		Co-doped TiO$_2$		Mn/Co doped TiO$_2$	
	Particle size, (nm) anatase / rutile	Phase content, f_A % anatase	Particle size, (nm) anatase / rutile	Phase content, f_A % anatase	Particle size, (nm) anatase / rutile	Phase content, f_A % anatase
0.02	38.2 / 0	100	44.3 / 0	100	-	-
0.04	39.4 / 0	100	40.4 / 0	100	-	-
0.1	38.7 / 0	100	40.1 / 0	100	40.1 / 0	100
0.3	40.6 / 0	100	37.5 / 0	100	38.6 / 0	100
1	31.1 / 53	86.5	43.5 / 48.7	50.4	-	-

479

480 **Table 2.**

481 Effect of Mn and Co dopant level on band gap.

Dopant concentration (molar ratio)	Mn-doped TiO$_2$ Indirect band gap (eV)	Co-doped TiO$_2$ Indirect band gap (eV)	Mn/Co-doped TiO$_2$ Indirect band gap (eV)
0.02	2.7	2.97	
0.04	2.85	2.85 [1.6*]	3 [1.6*]
0.1	2.75	2.83 [1.55*]	2.7 [1.5*]
0.3	2.6	2.7 [1.5*]	
1	2.4	2.4 [1.41*]	

482

483 * Sub-band gap

484

485 **Figure captions**

486 **Figure 1**

487 XRD patterns of a) Mn-doped TiO_2 (0.02-1 wt%), b) Co-doped TiO_2 (0.02-1 wt%) and c) Mn

488 & Co co-doped TiO_2 (binary dopant concentration range: 0.04-0.1 wt%).

489 **Figure 2**

490 UV-Vis absorption of P25 and a) Mn-doped TiO_2 (0.02-1 wt%), b) Co-doped TiO_2 (0.02-1

491 wt%) and c) Mn & Co co-doped TiO_2 (binary dopant concentration range: 0.04-1 wt%).

492 **Figure 3**

493 TEM images of a) Mn-doped TiO_2 (1 wt%) and b) Co-doped TiO_2 (1 wt%).

494 **Figure 4**

495 *E. coli* inactivation in the presence of different Mn- and Co-doped TiO_2 catalysts and the

496 commercially available TiO_2 (P25, Evonik). Catalyst concentration is 100 mg/L.

497 **Figure 5**

498 *K. pneumoniae* inactivation in the presence of different a) Mn- and b) Co-doped TiO_2

499 catalysts and the commercially available TiO_2 (P25, Evonik). Catalyst concentration is 250

500 mg/L.

501 **Figure 6**

502 *E. coli* and *K. pneumoniae* inactivation in the presence of Mn & Co co-doped TiO_2. Catalyst

503 concentration is 100 and 250 mg/L for *E. coli* and *K. pneumoniae* inactivation, respectively.

504 **Figure 7**

505 SEM images of *E. coli* (a-e) and *K. pneumoniae* (f-j) without treatment (negative controls)

506 and after photocatalytic treatment in the presence of metal-doped TiO_2.

507 **Figure 8**

508 Effect of initial bacterial concentration on disinfection efficiency for a) *E. coli* (conditions:

509 0.02 wt% Co, 100 mg/L) and b) *K. pneumoniae* (conditions: 0.3 wt% Mn, 250 mg/L).

510 **Figure 9**

511 Effect of photon flux and wavelength on the inactivation of a) *E. coli* (conditions: 0.1 wt%

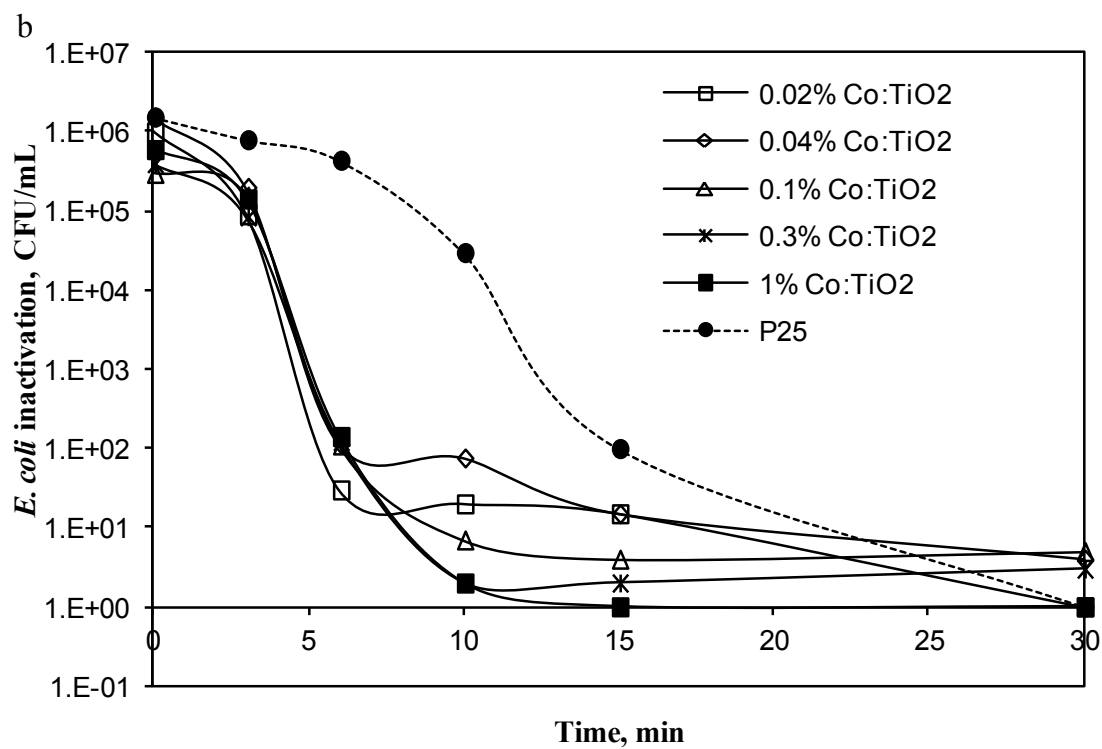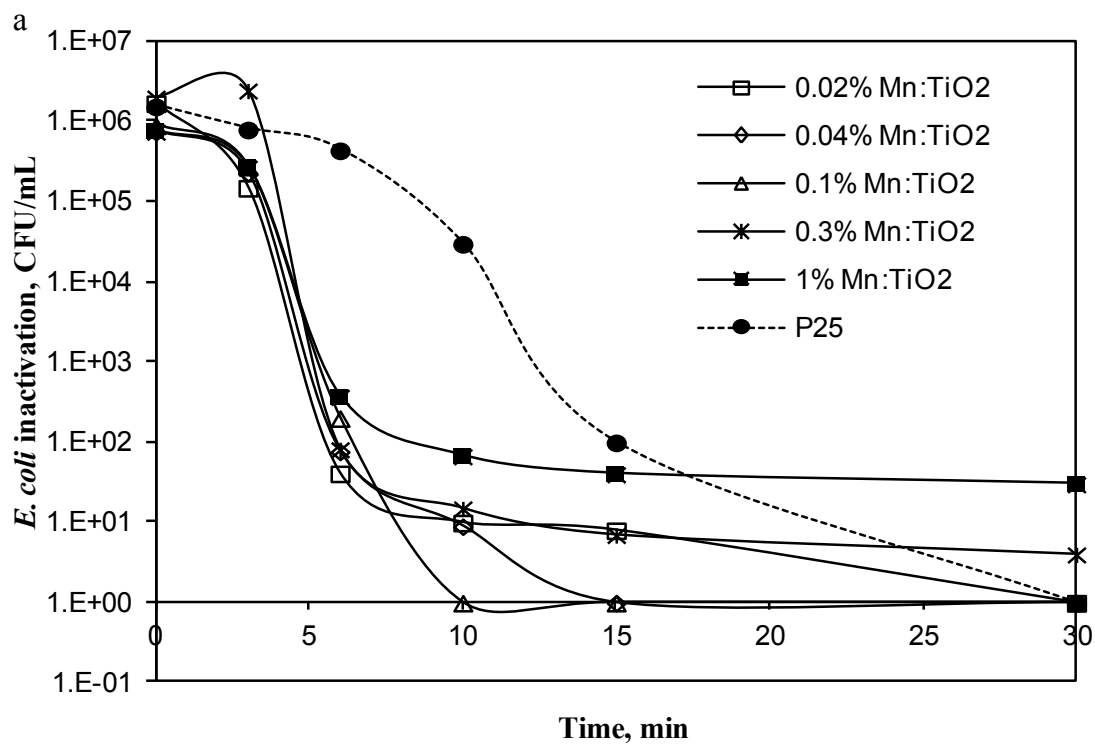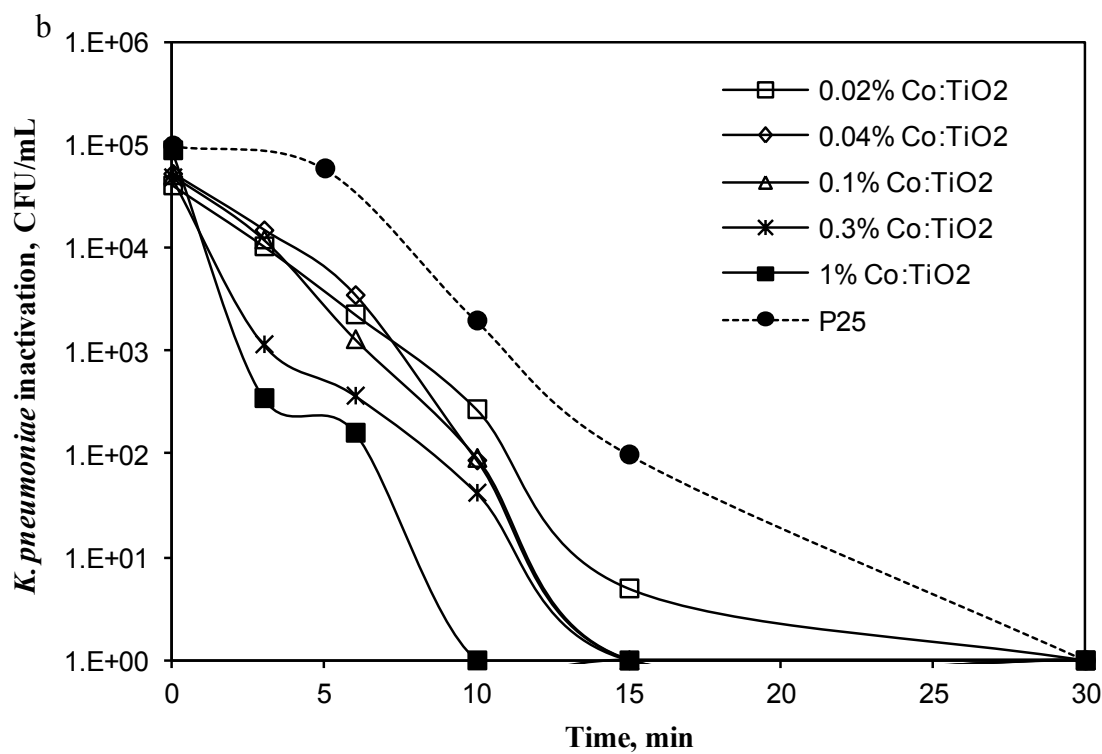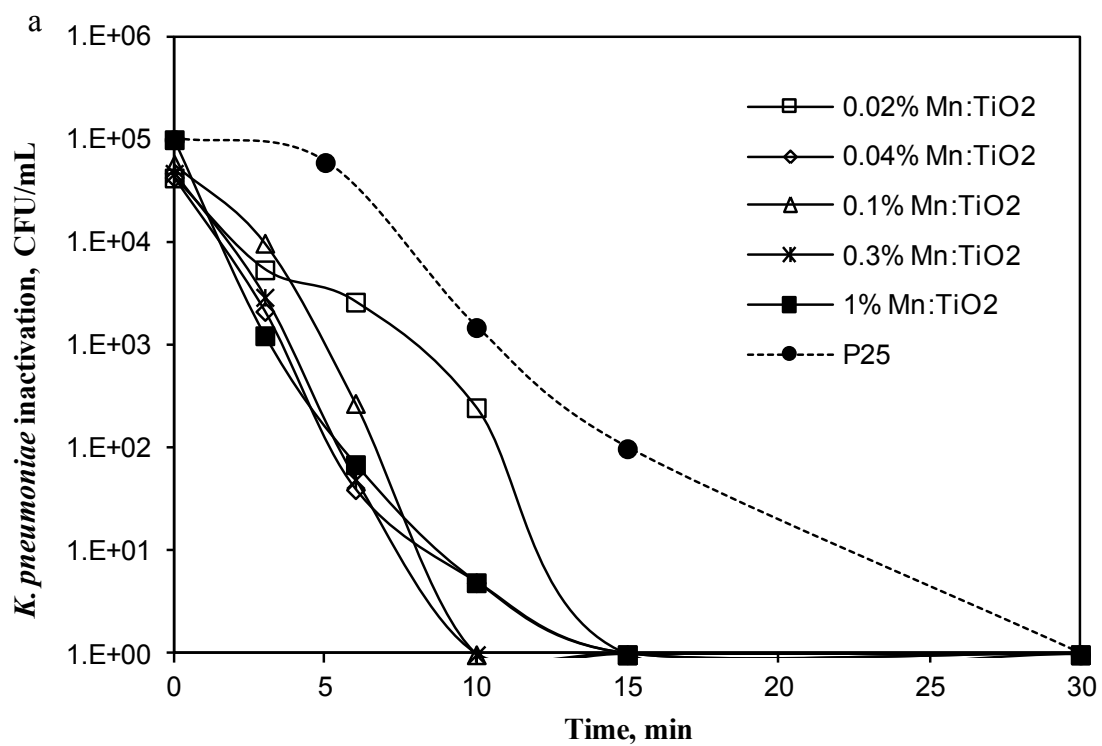512 Mn, 100 mg/L) and b) *K. pneumoniae* (conditions: 1 wt% Co, 250 mg/L).

513

Figure 1

517   **Figure 2**

519 **Figure 3**

Figure 4

a

b

Figure 5

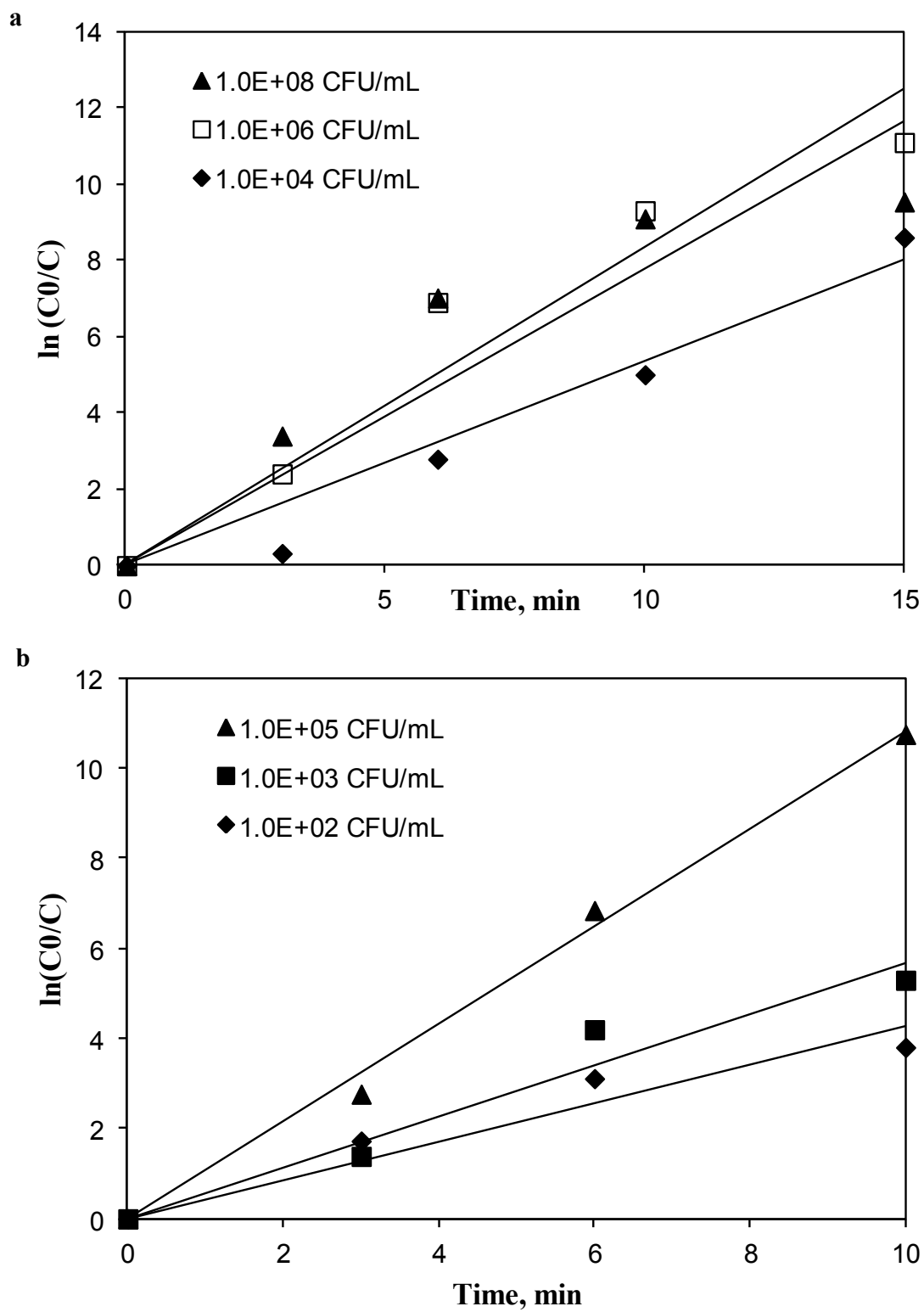**Figure 6**

Figure 7

32

531   **Figure 8**

534 **Figure 9**